Appl. Phys. B 70 [Suppl.], S67–S75 (2000) / Digital Object Identifier (DOI) 10.1007/s003400000307

Applied Physics B
Lasers
and Optics

Techniques for the characterization of sub-10-fs optical pulses: a comparison

L. Gallmann, D.H. Sutter, N. Matuschek, G. Steinmeyer, U. Keller

Ultrafast Laser Physics Laboratory, Institute of Quantum Electronics, Swiss Federal Institute of Technology, ETH Hönggerberg – HPT, CH-8093 Zürich, Switzerland
(Fax: +41-1/633-1059, E-mail: gallmann@iqe.phys.ethz.ch)

Received: 1 October 1999/Revised version: 29 February 2000/Published online: 24 May 2000 –

Abstract. Several methods have been proposed for the phase and amplitude characterization of sub-10-fs pulses with nJ energies. An overview of these techniques is presented, with a focus on the comparison of second-harmonic generation frequency-resolved optical gating (SHG-FROG) and spectral phase interferometry for direct electric-field reconstruction (SPIDER). We describe a collinear FROG variant based on type-II phase-matching that completely avoids the geometrical blurring artifact and use both this and SPIDER for the characterization of sub-10-fs Ti:sapphire laser pulses. The results of both methods are compared in an extensive statistical analysis. From this first direct experimental comparison of FROG and SPIDER, guidelines for accurate measurements of sub-10-fs pulses are derived. We point out limitations of both methods for pulses in this ultrashort pulse regime.

PACS: 42.65.Re; 42.60.Fc; 42.30.Rx

During the past decade, continuous progress in the field of ultrashort pulse generation has lead to pulse durations below 6 fs in the visible and near-infrared spectral range [1]. These ultrashort pulse durations have independently been generated with three different techniques, namely optical parametric amplification [2], compression in either single-mode fibers [3] or hollow optical waveguides [4], and, most recently, by direct generation in Ti:sapphire laser oscillators [5, 6]. Despite the variety of methods, all these sources exhibit broad and complex spectra, making characterization of their pulses a demanding task.

Conventional autocorrelation techniques, which require a priori knowledge of the pulse shape, can be used to determine rough estimates of the pulse duration. For a more precise measurement, a variety of methods has been proposed allowing for a full reconstruction of pulse amplitude and phase from measured data only [7–11]. Of these methods, especially frequency-resolved optical gating (FROG, [8, 12]) has found widespread use. Recently, two new methods have been introduced: spectral phase interferometry for direct electric-field reconstruction (SPIDER, [11, 13]) and iterative decorrelation of the second-order autocorrelation [14]. These three methods have also been used for the characterization of pulses in the sub-10-fs regime [3, 15–19]. The applicability of a particular measurement technique in this pulse duration regime is not solely determined by possible bandwidth limitations but also by the requirements on the nonlinear optical process or the beam geometry involved.

Currently, research to produce pulses of even shorter duration is underway. While it is speculated that pulses from existing sources of high-harmonic generation exhibit attosecond time signature, pulse characterization methods have yet to be demonstrated in the sub-fs regime. This shows that measurement of extremely short pulses can be as much of a challenge as the generation of the pulses themselves. In this paper, we will give an overview of two phase-sensitive pulse characterization methods that are suitable for the optical two-cycle regime and beyond. We investigate systematic limitations of the characterization techniques. Based on measurements on a SESAM-assisted Kerr-lens modelocked Ti:sapphire laser [6], we directly compare FROG, SPIDER, and interferometric autocorrelation.

1 Motivation for amplitude and phase characterization

Until recently it was the accepted standard that pulse duration is determined with autocorrelation measurements. The temporal parameters have usually been obtained by fitting an analytical pulse shape with constant phase to an autocorrelation measurement. The particular fitting function is motivated by theoretical models of the pulse formation process. For passively modelocked lasers, for example, that allow for parabolic approximation of these formation mechanisms one expects a sech^2 temporal and spectral pulse shape [20]. For lasers obeying such a model the a priori assumption of a theoretically predicted pulse shape is well-motivated and leads to good estimates of the pulse duration as long as the measured spectrum also agrees with the theoretical prediction. Passively modelocked solid-state lasers with pulse durations well above 10 fs normally generate pulses close to the ideal sech^2 shape [21, 22]. Therefore, autocorrelation is still a good standard diagnostic for such laser sources.

In the sub-10-fs regime, however, theoretical models have to consider higher order effects and thus become more complicated. In this case, no simple analytical pulse shapes can be expected. Experimentally, this situation is clearly indicated by more complex pulse spectra, deviating from the ideal sech^2 shapes predicted by the simpler models [6, 23–26]. Additionally, even after dispersion compensation, broadband pulses usually exhibit an uncompensated chirp. Chirped mirrors, for example, lead to a sinusoidal modulation of the spectral phase that cannot be completely compensated for by conventional techniques. Although close to the transform limit, such pulses are distorted by the uncompensated phase structure (see for example [18, 19]).

Figure 1 shows the measured interferometric autocorrelation of a pulse with a transform limit of 5.3 fs. We compare this data to an analytical sech^2 fit and autocorrelations calculated from SPIDER measurements of the same pulse. The sech^2 fit yields a pulse duration of 4.5 fs, but cannot account for the pedestals of the autocorrelation. In general, any fit neglecting the complicated spectral and phase structure of such broadband pulses will lead to erroneous results. We observed the tendency of such fits to underestimate the true duration of the pulses. On the other hand, the pulses retrieved from the SPIDER measurements with a 30% longer duration agree excellently with the measured autocorrelation data presented in Fig. 1. However, it is important to note that this good agreement is necessary but not sufficient to confirm the accuracy of the pulse characterization. For example, we typically observe with our sub-10-fs Ti:sapphire laser that the interferometric autocorrelation does not change as much as the SPIDER or FROG measurements when we change the extracavity dispersion. Thus, this discussion should demonstrate that even for determining the duration of a pulse, amplitude and phase sensitive characterization techniques are mandatory in the sub-10-fs regime.

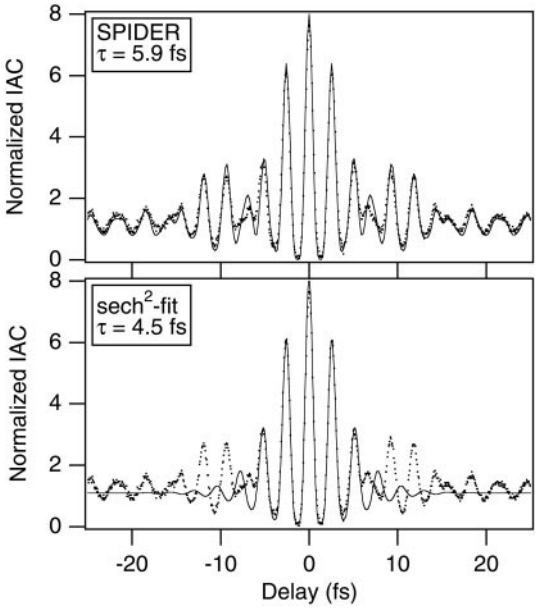

Fig. 1. Measured interferometric autocorrelation of a pulse with a 5.3-fs transform limit (*dots*). This data is compared to a theoretical sech^2-fit (*bottom*) and to the autocorrelations calculated from a SPIDER measurement (*top*)

New methods developed for a full pulse characterization, such as SPIDER and FROG, have also been used for time-resolved spectroscopy where the phase information resulted in additional insight into the microscopic physics. The knowledge of the full complex electric field is clearly needed to get all the information contained in a signal beam (for example [27, 28]). We also have demonstrated that the differential transmission response of semiconductors excited well above the band edge with 20-fs pulses can be manipulated by the phase of the broadband excitation and readout pulses [29, 30]. Furthermore, coherent control uses the amplitude and phase of the laser light to manipulate the quantum mechanical phase relationships among the eigenstates of matter [31–33]. More recently, this has been used to control chemical reactions [34].

2 SHG-FROG in the sub-10-fs regime

2.1 Noncollinear FROG and the geometrical blurring artifact

Frequency-resolved optical gating (FROG) is a characterization method based on the measurement of a spectrally resolved autocorrelation signal followed by an iterative phase-retrieval algorithm to extract the intensity and phase of the laser pulse. FROG has been used for pulse durations from few femtoseconds to several picoseconds and for pulse energies ranging from the nJ- to the mJ-regime. For a more general overview of the FROG technique, the reader is referred to [12, 35]. The nJ pulse energies of our laser dictate that we use second-harmonic generation FROG (SHG-FROG, [35]). Consequently, the discussion will focus on this FROG variant.

In the sub-10-fs range, two serious problems with the FROG technique arise. The first is bandwidth limitation of the optics and the detection system involved, in particular the bandwidth limitation of the SHG process. This problem is reduced by using extremely thin nonlinear optical crystals. In contrast to autocorrelation, FROG allows us to correct for bandwidth limitations to a certain extent. With this correction, measurements of 4.5-fs pulses have been successfully demonstrated [15, 36]. Still, particular care has to be given to the accurate determination of the spectral calibration of the setup.

A second more fundamental limitation is the reduction of temporal resolution caused by the finite beam-crossing angle in the nonlinear crystal. Unlike sub-10-fs autocorrelators, a noncollinear geometry is conventionally used for FROG measurements. In the noncollinear geometry, temporal resolution has to be traded for suppression of interference fringes. Assuming Gaussian spatial and temporal profiles, ideal phase matching, and small crossing angles θ_0 the temporal resolution δt is given by

$$\delta t = \theta_0 \frac{w_0}{c}\,, \tag{1}$$

where w_0 is the beam radius in the focal plane and c the speed of light [36, 37]. Now, θ_0 has to be chosen according to the required suppression of interferences in the recorded FROG trace. The apparent duration τ_M retrieved from a distorted FROG trace is related to the effective pulse duration τ_P

by

$$\tau_{\mathrm{M}}^2 = \tau_{\mathrm{P}}^2 + \delta t^2 \,. \tag{2}$$

For ideal spatial beam profiles, the product of far-field angular spread and the near-field spot size w_0 is a constant and depends only on wavelength. This relation dictates the minimum acceptable choice of θ_0 in (1). In [36], an ultimate temporal resolution of $\delta t = 0.4$ fs at a center wavelength of 800 nm has been estimated for noncollinear SHG-FROG, assuming an overlap of the beams at the $1/\mathrm{e}$ points in the far field. Experimentally, however, an angle significantly larger than this has to be chosen to avoid detrimental interference effects in the recorded FROG trace. This results in temporal resolutions δt larger than about 1.5 fs [16, 37]. Spatial beam distortions and poor focusability, more often observed with ultrashort pulses, may require that θ_0 has to be increased further to achieve the same amount of interference rejection and may result in an increased beam radius w_0 in the focal plane [38].

The geometrical blurring artifact can be reduced by suitable aperturing of the SHG-FROG signal in the near-field. With aperturing, selection of the center part of the signal reduces geometrical smearing, but also reduces signal strength. Aperturing has to be done with care to avoid delay-dependent spectral shaping [36]. Another option to reduce geometrical blurring would be to use a collinear type-I FROG setup. In this case, an excessive number of spectra would need to be acquired to properly resolve the interference fringes. The interference fringes would require either a special phase-retrieval algorithm or removal by Fourier filtering, which would again affect the temporal resolution. At present, we are not aware of any successful demonstration of a collinear type-I FROG apparatus.

2.2 Collinear type-II SHG-FROG

As an alternative approach we use a collinear geometry in combination with type-II phase matching to solve the problems associated with the geometrical blurring artifact. Type-II second-harmonic generation is attractive because there is no need to modify the algorithms originally developed for noncollinear type-I SHG-FROG. Collinear type-II SHG-FROG was first demonstrated as a valuable tool for the characterization of ultrashort pulses in the focus of a microscope objective [39, 40]. With a setup modified for the measurement of sub-10-fs pulses we characterized pulses with a transform limit as short as 5.3 fs and a pulse duration of 6.6 fs [18]. Figure 2 shows the setup used in our experiments. The 6.6 fs-pulses measured with this FROG variant are displayed in Fig. 3.

The most important consideration for a type-II setup is the minimization of polarization-dependent spectral shaping in the two perpendicularly polarized beam paths. This shaping effect can give rise to asymmetry in the autocorrelations or the FROG traces. With a sufficiently thin nonlinear crystal, the dominant sources of asymmetry are the beamsplitters. Using near-normal incidence on the beamsplitters avoids this problem.

With the extremely thin nonlinear crystals required for the measurement of sub-10-fs pulses, additional non-phase-matched processes may contribute spurious SHG signals, interfering with the type-II FROG signal. For a 10-μm-thick BBO crystal (point-group $3m$) one spurious signal is generated via the square nonlinearity tensor element d_{31} [41]. This signal is polarized along the extraordinary axis and therefore results in a distortion of the FROG trace. For our setup we chose a 10-μm-thick ADP crystal (point-group $\bar{4}2m$). Because of the higher crystal symmetry, the only second-harmonic background signal present with ADP stems from the d_{25} tensor element. Because it is polarized perpendicularly to the FROG signal, it is easily rejected by a polarizer.

The major limitation of the temporal resolution of a collinear type-II SHG-FROG apparatus is the group-velocity-mismatch (GVM) in the nonlinear crystal. GVM between the orthogonally polarized fundamental pulses causes a temporal blurring of the FROG-data similar to the geometrical

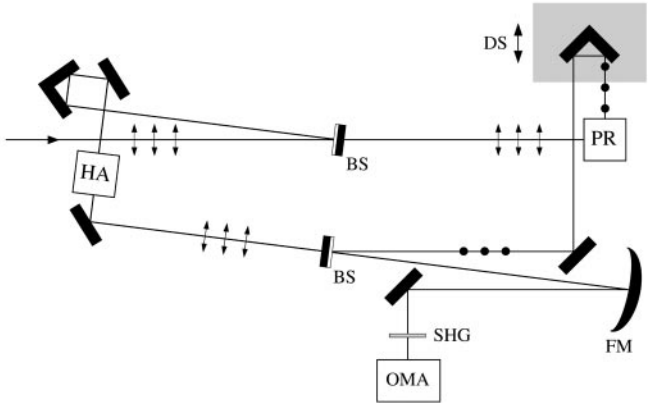

Fig. 2. Collinear type-II SHG-FROG setup: BS = beamsplitters, PR = periscope for polarization rotation, HA = periscope for height adjustment, FM = focusing mirror, SHG = nonlinear crystal, OMA = optical multichannel analyzer. *Dots* and *arrows* on the beam path display the polarization state of the beam

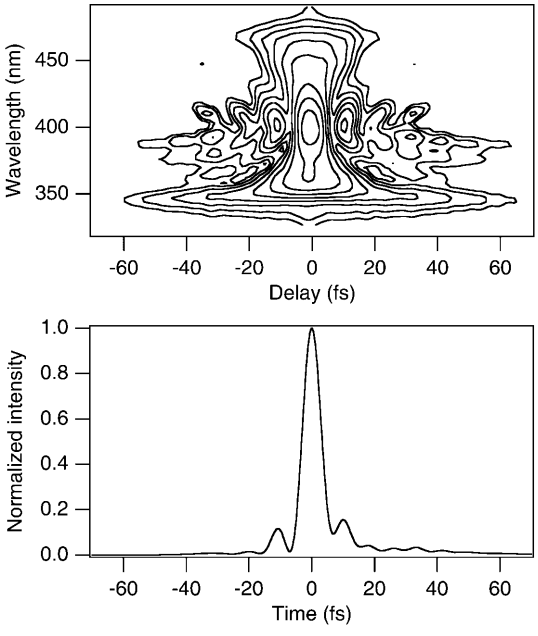

Fig. 3. Collinear type-II SHG-FROG measurement of 6.6-fs pulses. The recorded FROG trace (*above*) and the retrieved temporal intensity profile (*below*) are shown

blurring in a noncollinear setup. For the collinear type-II apparatus, however, the temporal resolution is independent of beam quality. Additionally, a collinear setup does not require careful alignment and control of the beam crossing angle to achieve optimum temporal resolution. For a 10-μm-thick ADP crystal, GVM between the fundamental pulses amounts to 1.2 fs. Although not strictly analogous to δt defined in (1), this number is on the order of the best reported values of geometrical beam-smearing in noncollinear setups [16, 36, 37].

2.3 Spectral calibration and frequency-dependent mode-size

Because FROG reconstructs the pulse profile from a series of second-harmonic spectra, spectral calibration errors may cause distortions of the reconstruction algorithm. Therefore, it is mandatory to correct for spectrally varying second-harmonic generation and signal detection efficiencies of broadband FROG measurements. The efficiency of second-harmonic generation can be calculated from known crystal parameters. Following [36] and the assumptions therein, the type-II conversion efficiency is

$$R(\Omega, L) = \frac{\Omega^2}{n_\mathrm{e}(\Omega)} \times \left[(n_\mathrm{e}^2(\Omega) - 1) \left(n_\mathrm{e}^2 \left(\frac{\Omega}{2} \right) - 1 \right) \left(n_\mathrm{o}^2 \left(\frac{\Omega}{2} \right) - 1 \right) \right]^2 \times \mathrm{sinc}^2 \left(\frac{\Delta k(\Omega) L}{2} \right) , \tag{3}$$

with Ω representing the second-harmonic frequency, n_e and n_o the refractive indices of the extraordinary and the ordinary axes, respectively, Δk the phase mismatch, and L the crystal length. The measured FROG trace $S(\Omega, \tau, L)$ is related to the corrected trace $S^{\mathrm{SHG}}_{\mathrm{FROG}}(\Omega, \tau)$ by

$$S(\Omega, \tau, L) \propto Q(\Omega) R(\Omega, L) S^{\mathrm{SHG}}_{\mathrm{FROG}}(\Omega, \tau) . \tag{4}$$

The detection efficiency $Q(\Omega)$ is measured using a calibrated white-light source.

Compared to [36], a factor of Ω that accounts for the frequency-dependent mode-size (FDMS) has been omitted in (3). Using a set of 10-nm-wide interference filters, we monitored the change in FDMS in the focal plane of our FROG setup with slight variation in intracavity dispersion (see Fig. 4). In our measurements on the sub-10-fs oscillator, we did not observe the simple relationship, suggested in [36], that relies on the assumption of a linear optical cavity. Instead, we observe a complex behavior of the FDMS with strong spectral variations. At particular wavelengths, we observe more than 50% difference in the FDMS between the two data sets displayed in Fig. 4, with only a few 10 μm change in intracavity prism insertion. It has been suggested earlier that the FDMS of a Kerr-lens modelocked (KLM) Ti:sapphire laser is determined by the interplay between the Kerr nonlinearity and the intracavity dispersion [42]. Therefore, the FDMS depends strongly on the particular pulse shape [43]. It should be pointed out that this dependence is a particular property of a KLM laser and is not expected to be relevant for other sources of sub-10-fs pulses. In our measurements, we find

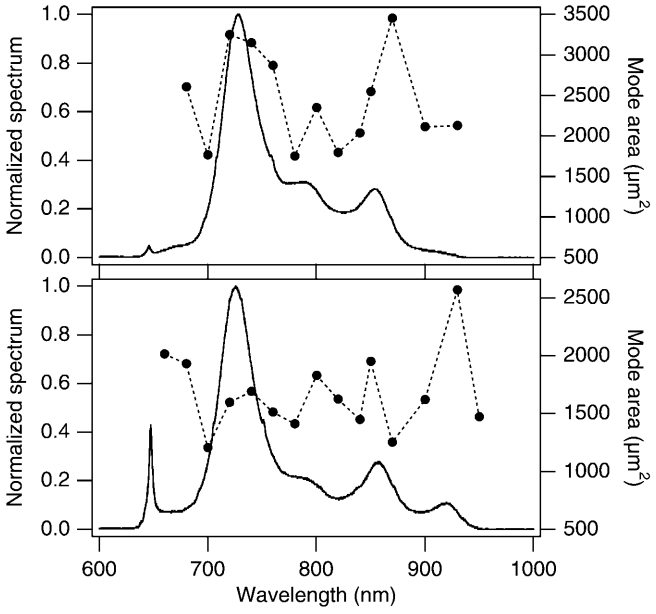

Fig. 4. Measured frequency-dependent mode size. Mode areas (*filled circles*) for two different intracavity dispersion values are shown. Local maxima in the mode size coincide with local maxima of the corresponding pulse spectrum (*solid line*). Qualitatively different types of frequency-dependencies have been observed for different intracavity dispersion

that completely omitting the FDMS factor in (3) better approximates the data as displayed in Fig. 4.

A strong FDMS manifests itself as a deviation of the frequency marginal ([44], FROG trace integrated along delay axis) from the autoconvolution of the fundamental spectrum. Since in the nonlinear crystal all the modes present in the input beam are mixed in a convolution-like manner, in general, the FDMS-effect can not easily be corrected for in the FROG data. For some special but rather common cases, however, such a correction can and should be done [36].

2.4 Discussion of the SHG-FROG technique

One problem with using the FROG technique in the sub-10-fs regime is the extremely wide bandwidth associated with such short pulses. A strong spectral sensitivity dependence effectively reduces the dynamic range of the detection system and may lead to increased noise in the spectral wings. To guard against such spectral distortions and other systematic errors in the data, FROG provides the FROG marginals [44]. Another issue closely connected to the presence of noise in the data is the problem of the convergence of the phase-retrieval algorithm. For FROG traces of complicated structure the presence of excessive noise may cause early stagnation of the optimization algorithm in a non-optimal local minimum. The particular importance of noise issues together with the complex pulse structures observed in the sub-10-fs regime often results in slow convergence of the retrieval algorithm and makes fast update rates virtually impossible. For amplified laser systems, however, inversion of SHG-FROG traces of longer pulses have been demonstrated at multi-Hertz refresh rates [45].

So far, noncollinear SHG-FROG has been demonstrated with pulses as short as 4.5 fs [15]. For pulses significantly

shorter than that, the geometrical blurring artifact must be corrected either directly in the phase-retrieval algorithm or with aperturing. To some extent, our collinear implementation uses a much simpler setup, unrestricted by geometry. However, serious problems are expected in a type-II setup as soon as fundamental and SHG spectrum overlap. In this case, in contrast to type-I geometries, the fundamental light cannot be fully rejected by means of polarization. Thus, if such broad spectra have to be characterized with SHG-FROG, type-I geometries must be used exclusively. A collinear type-I FROG setup with a suitably modified retrieval algorithm provides a promising solution by combining the absence of the geometrical smearing with less restrictive bandwidth limitations. Another option would be to account for the geometrical smearing effect in the retrieval algorithm as a noninstantaneous response of the nonlinear medium [46]. Both methods should allow for an accurate FROG characterization of pulses in the single-cycle regime.

3 SPIDER

SPIDER is a self-referencing variant of spectral interferometry [11, 13]. Conventional spectral interferometry measures the spectral phase differences between two pulses [47]. To access the spectral phase of a single pulse, SPIDER generates a spectral shear between the carrier frequencies of two replicas of this pulse. The phase information of the resulting interferogram allows the direct reconstruction of the spectral phase of the input pulse.

The spectral shear is generated by upconversion of the two replicas with a strongly chirped pulse using sum-frequency generation in a nonlinear optical crystal. It is convenient to directly derive the chirped pulse from the pulse to be measured by a dispersive element. The upconverter pulse has to be stretched such that its instantaneous frequency can be considered constant for the duration of the pulse to be measured. Being separated by a delay τ much longer than the pulse duration, the two replicas are upconverted by different portions of the chirped pulse with different frequencies. The resulting spectral interference pattern of the upconverted short pulse replicas is of the form

$$S(\omega) = |E(\omega)|^2 + |E(\omega+\delta\omega)|^2 + 2|E(\omega)E(\omega+\delta\omega)| \times \cos[\phi(\omega+\delta\omega) - \phi(\omega) + \omega\tau]\,, \quad (5)$$

where $E(\omega)$ is the frequency-domain representation of the electric field, $\phi(\omega)$ the spectral phase of the input pulse, ω denotes the angular frequency and $\delta\omega$ the spectral shear. The phase information contained in the cosine term of (5) can be extracted by a non-iterative, purely algebraic method [48]. The constant delay τ is determined once by spectral interferometry of the two short-pulse replicas. After subtraction of the linear phase term $\omega\tau$, one obtains the spectral phase $\phi(\omega)$ at evenly spaced frequencies $\omega_i = \omega_0 + i \times \delta\omega$ by adding up the phase differences $\phi(\omega_n + \delta\omega) - \phi(\omega_n)$ $(n = 0..i-1)$. In a final step, the complex frequency domain representation of the electric field of the pulse is obtained from the reconstructed spectral phase and an independent measurement of the power spectrum. Temporal profiles are obtained by Fourier transforming these results. Recently, a method for recording the fundamental pulse spectrum and the SPIDER interferogram simultaneously has been demonstrated [49].

Inaccuracies in the determination of the linear phase associated with the delay τ show up as errors in the reconstructed phase $\phi(\omega)$. Such inaccuracies can be caused by differences between the wavelength calibration used for the measurement of the linear phase and the one used for the measurement of the SPIDER interferogram. These problems are suitably avoided if the linear phase is derived from the SHG of the two pulse replicas rather than from their fundamental. This allows using the same calibration for the SPIDER and the linear phase data and cancels out most of the calibration errors in the process of subtracting the linear phase from the SPIDER interferogram phase [50].

SPIDER is an intrinsically fast technique. It requires acquisition of only two spectra and the pulse reconstruction consists of two Fourier transforms executed in the fraction of a second on a modest computer. SPIDER has been demonstrated for real-time single-shot characterization of a 10-Hz amplifier system and with update rates as fast as 20-Hz for a 1 kHz amplifier system [51, 52]. SPIDER is particularly well suited for sub-10-fs pulse characterization for several reasons. In this regime, a short piece of a highly dispersive glass is sufficient for the generation of the strong chirp of the upconverter pulse. Use of sum-frequency mixing results in a more economic use of detection bandwidth, compared to SHG-based techniques. We have used SPIDER to characterize pulses with nJ energy, a transform limit of 5.3 fs, and a duration as short as 5.9 fs [19]. In the following subsection we discuss the SPIDER setup optimized for the sub-10-fs range.

*3.1 Sub-*10-fs *SPIDER setup*

The SPIDER apparatus optimized for the sub-10-fs regime is shown in Fig. 5. The major part of the input beam is directed through an uncoated 6.5-cm-long SF10 glass block to generate the chirped pulse for the upconversion. The Fresnel reflection from the first surface of this glass block also serves as a broadband beamsplitter. After the all-reflective polarization rotation, the two pulse replicas are generated in a Michelson-interferometer with balanced reflectivity and dispersion. The interferometer uses broadband dielectric beamsplitters on 300-μm substrates. The two pulse replicas are noncollinearly mixed with the beam from the dispersive arm in a 30-μm-thick BBO crystal cut for type-II interaction. The advantage of the noncollinear mixing geometry is that no additional beamsplitter is needed for beam recombination. Both the geometrical blurring effect caused by the noncollinear beam geometry and GVM do not play a role in SPIDER because the upconversion pulse is strongly stretched and can be treated as cw-radiation within the time frame defined by the input pulse. Additionally, the quasi-cw nature of the upconversion beam is exploited in a type-II interaction by polarizing the stretched pulse along the low-bandwidth extraordinary crystal axis. In this axis, only a bandwidth given by the spectral shear $\delta\omega$ is required. This allows using the large-bandwidth ordinary axis for the short-pulse replicas and significantly extends the useable bandwidth in comparison with a type-I process in the identical nonlinear material.

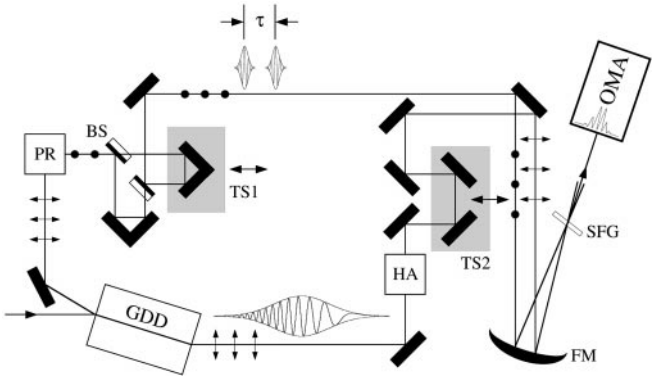

Fig. 5. SPIDER setup: GDD = glass block for pulse stretching, PR = periscope for polarization rotation, BS = beamsplitter, TS1 = translation stage for adjustment of delay , HA = periscope for height adjustment, FM = focusing mirror, SFG = nonlinear crystal, OMA = optical multichannel analyzer, TS2 = translation stage for adjustment of overlap with upconverter pulse. *Dots* and *arrows* on the beam path display the polarization state of the beam

It is possible to build a SPIDER apparatus without the need for coated beamsplitters by replacing the Michelson interferometer with a very thin etalon before the glass block [52]. The two delayed short-pulse replicas are generated by Fresnel reflection from the first and the second etalon surface. The advantages of this approach are easier alignment, better stability, and very large bandwidth. In fact, the bandwidth of such a SPIDER apparatus would be limited only by the nonlinear crystal, whose bandwidth can be much larger than that of dielectric beamsplitter coatings.

3.2 Discussion of the SPIDER technique

For retrieving the spectral phase from a SPIDER measurement, no correction for the spectral sensitivity is required. This is true as long as the detection efficiency varies slowly with frequency compared to the interference period τ^{-1} which in most cases poses no restriction. This insensitivity towards calibration errors makes SPIDER a particularly attractive technique in the sub-10-fs regime. Of course, if the full reconstruction of the temporal pulse shape is desired, a sensitivity correction of the independently measured pulse spectrum is still needed. Systematic errors in a SPIDER measurement can be detected by measuring a pulse before and after propagation through a material with known dispersion. To properly resolve all the fringes of a SPIDER interferogram a more sophisticated spectrometer than with FROG is required. In our case, a 0.5-nm resolution is needed for the wavelength range from 350 nm to 450 nm.

Spectra covering a full octave pose no fundamental limitation to the SPIDER technique since the generated sum frequency signal is geometrically separated from both fundamental beams. Stray light of the fundamental pulse replicas can be reduced by use of a polarizer, whereas stray light from the upconverter pulse adds to an unmodulated background. Strong spectral phase variations might result in a fringe spacing beyond the resolution of the spectrograph. The spectral resolution therefore determines an upper limit for the chirp that can be measured with SPIDER.

4 Experimental comparison of SHG-FROG and SPIDER

For a fair experimental comparison of collinear type-II SHG-FROG and SPIDER, we aligned our Ti:sapphire laser for optimum long-term stability to keep fluctuations at an absolute minimum. This requires operating the laser slightly farther away from the stability limit and at a longer pulse duration. For the experiments described in this section, the laser exhibited a transform limit of 7.4 fs. Under these conditions, we recorded 10 independent measurements with both techniques. The FROG traces were recorded at a 1.46-fs step size and a spectral resolution of 1.1 nm. The data is arranged on a (128 × 128)-grid. All traces were corrected according to Sect. 2.3. For pulse-retrieval, commercial software (Femtosoft Technologies) was used and 600 iterations of the algorithm were used to ensure convergence. The SPIDER data were acquired with a spectral resolution of 0.27 nm. The delay of the short-pulse replicas was 302 fs, resulting in a spectral shear of $0.029\,\mathrm{fs}^{-1}$. The group delay dispersion in the dispersive SPIDER arm was $10\,400\,\mathrm{fs}^2$. For phase retrieval from the interferogram we used the procedure described in [48].

Even though SPIDER can acquire data more rapidly, we deliberately used the same time span for each set of measurements to keep laser drift at a comparable magnitude. Moreover, the two setups were designed to have nearly identical dispersion. However, due to the very short pulse duration, even small deviations caused by slightly unequal air paths became noticeable. We attribute slight differences between the results obtained with the two techniques mostly to unequal dispersion in the beam paths. Additionally, systematic errors of one or the other method may contribute.

We also performed independent consistency checks by visually comparing the retrieved pulses with simultaneously recorded interferometric autocorrelations (Fig. 6). The agreement between the the measured data and the autocorrelations calculated from the retrieved pulses is excellent, as was observed in earlier crosschecks performed on shorter pulses (see Fig. 1 and [18, 19]). From these checks, we expect systematic errors to be relatively small for both techniques. For the pulses displayed in Fig. 6, the use of FROG and SPIDER result in a pulse duration of about 9 fs, whereas fitting a sech^2 pulse shape to the experimental autocorrelation yields a pulse duration of 7.5 fs. As discussed in Sect. 1, the assumption of a particular pulse shape can lead to large errors in the estimation of the pulse duration. Often, this tendency is indicated by the strong deviations of the spectral shape from a sech^2 shape. The same arguments hold for the a priori assumption of other analytical pulse shapes.

Having discussed potential sources of systematic errors in the previous sections, we now turn to the statistical errors characteristic of the individual techniques. For this discussion we use the complete set of 10 measurements and, additionally, a selected subset of 5 measurements. For FROG this selection is based on the FROG error, for SPIDER the first 5 measurements are chosen. The complete set of FROG measurements displays FROG errors ranging from 0.0032 to 0.0054. In the selection, no FROG error exceeds the value of 0.00375.

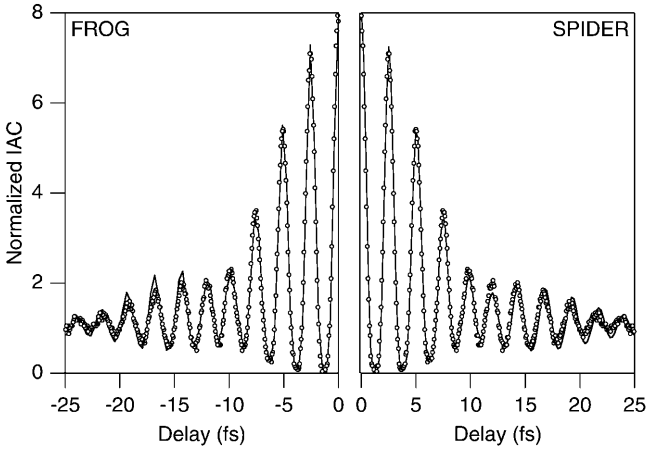

Fig. 6. Interferometric autocorrelations calculated from the retrieved pulses (*solid lines*) and the independently measured data (*circles*). Only one half of the autocorrelation is shown to better resolve the details of the traces. The result obtained from the FROG measurement is shown on the *left* and the data reconstructed with the SPIDER method are plotted on the *right*

4.1 Statistics of the temporal pulse parameters

Figure 7 contains temporal intensity profiles reconstructed with both FROG and SPIDER. The strongest fluctuations are present in the FROG evaluation with the full statistical set. One trace strongly deviates from all other measurements in the wings and this trace also corresponds to the highest FROG error. In the subset with the five lowest FROG errors, statistical fluctuations are strongly reduced. From this observation we conclude that the FROG error is well suited to compare the quality of FROG reconstructions taken at identical conditions. However, the FROG error might be a misleading criterion for a more general comparison of measurements because it depends on the grid size of the FROG trace as well as on the percentage of the grid being covered by the actual FROG data.

The statistical errors in the pulse profiles retrieved by SPIDER are comparable to those of the specially selected subset of FROG data. Restricting the evaluation to the first five SPIDER measurements results in a slight reduction of statistical fluctuations. This suggests a small but systematical temporal drift in the SPIDER data, which may be attributed either to a drift of the laser system or of the SPIDER apparatus itself. The greater fluctuations of the FROG setup prohibit the observation of such a small drift.

We compare the results of the FROG and SPIDER measurements in terms of the full width at half maximum (FWHM) duration of the temporal intensity profile. This disregards a lot of the information in Fig. 7, and the pulse duration turns out to be relatively insensitive to phase fluctuations. Averaging over the complete set of 10 measurements, we obtain a duration of 8.92 ± 0.23 fs with FROG and a pulse duration of 8.91 ± 0.11 fs with SPIDER. The pulse duration derived from both methods is in excellent agreement.

4.2 Statistics in the spectral domain

Figure 8 displays the pulse spectra reconstructed with the FROG technique. Significant deviations from the independently recorded pulse spectrum are observed, especially in the modulated center part of the spectrum. Again, the agreement with the independently recorded spectrum is improved when the subset with the lowest FROG errors is used. In this subset the agreement of the average of the reconstructed spectra with the actual pulse spectrum is excellent whereas the individual spectra still differ in shape. These differences are significantly larger than the spectral fluctuations of the laser system. Therefore, we attribute the variations to a low robustness of the reconstructed spectra against experimental noise. A similar comparison for the SPIDER technique is not applicable because the spectrum is not extracted from the interferogram but is measured separately.

Figure 9 contains a plot of the average spectral phase determined by each technique for each set of measurements. The error bars represent standard deviations. To estimate the correlation between spectral power density and phase error, the independently measured pulse spectrum is included in each graph.

Similar to the discussion in the previous section, the full set of FROG measurements shows the strongest fluctuations,

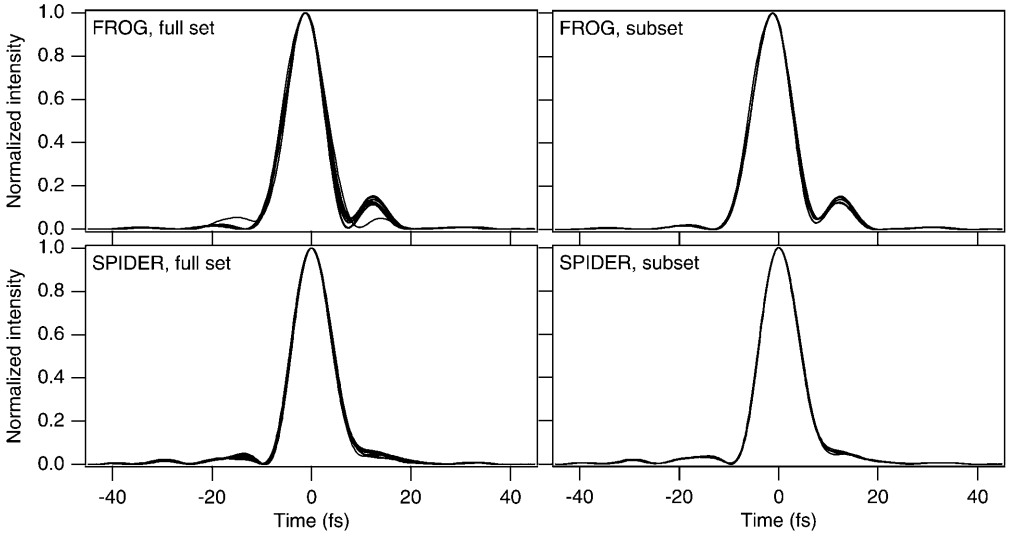

Fig. 7. Temporal intensity profiles reconstructed with FROG and SPIDER. On the *left side* all 10 measurements are shown. The *right side* displays the 5 measurements of the subsets

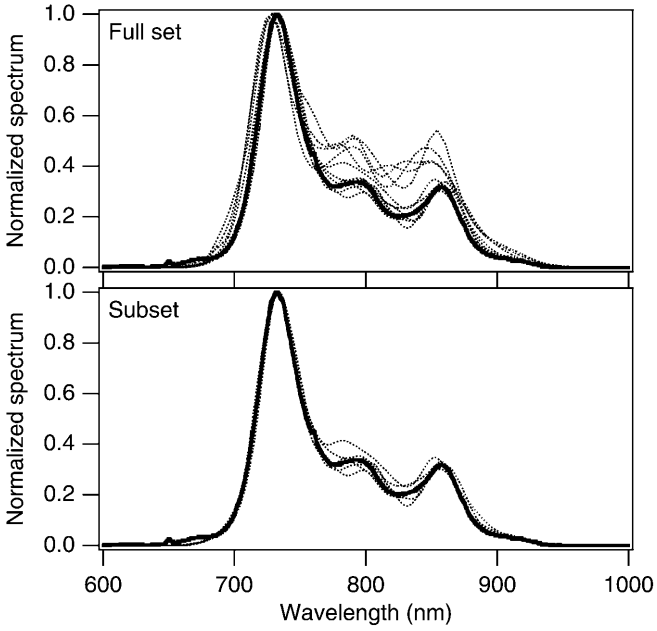

Fig. 8. Comparison of the FROG-reconstructed pulse spectra (*dashed curves*) with the independently measured pulse spectrum (*solid line*). Note the strong variations between the different FROG measurements

mainly due to one measurement. This is also the only case where signal strength and error bars appear to be uncorrelated. Selection of the subset results in a reduction of the fluctuations, in case of both measurement methods. For SPIDER, this reduction is strongest on the high frequencies, thereby indicating a temporal drift in this portion of the spectrum.

For a quantitative comparison of the phase measurements, we calculated the average of the standard deviations using the power spectrum as a weighting function. For the FROG technique we obtain an averaged statistical phase error of 0.122 rad for the full set and of 0.048 rad for the reduced set of measurements. For SPIDER the corresponding values are 0.044 rad and 0.017 rad. For phase measurements, SPIDER outperforms FROG by a factor of 3. The higher accuracy of SPIDER for spectral phase measurements can be understood from the fact that it is an interferometric technique that directly measures this quantity.

In our experiments, we observed that a small number of FROG measurements showed very poor convergence, giving rise to the outliers mentioned above. One obvious explanation for these poorly converging data sets is the much longer acquisition time required for multi-shot FROG. For a single FROG trace, 128 spectra are recorded and temporal drift of the laser might result in a slight inconsistency of the data acquired. In contrast, the data required for the SPIDER technique can be recorded in a single measurement on a CCD array.

5 Conclusion

We have presented an extensive discussion of SHG-FROG and SPIDER, two methods for the measurement of sub-10-fs pulses with nJ energy. The results for multi-shot SHG-FROG and SPIDER presented in this paper also apply to higher energy pulses in the sub-10-fs pulse duration regime. Even the shortest pulses currently available in the visible and near-infrared can be accurately characterized with the methods discussed in this paper.

FROG is very well established and provides several internal consistency checks. Specialized FROG techniques have been demonstrated for higher-pulse energies, single-shot variants, and setups that allow cross-correlation of pulses. FROG combines the accuracy of a state-of-the-art pulse measurement technique with the simplicity and the familiarity of a conventional autocorrelator.

For our application, the characterization of very short pulses close to the transform limit, we favor the SPIDER technique. In general, we find SPIDER easier to implement and more robust. SPIDER allows for fast acquisition and its spectral phase reconstruction is insensitive to spectrally varying detection and conversion efficiencies. Another attractive

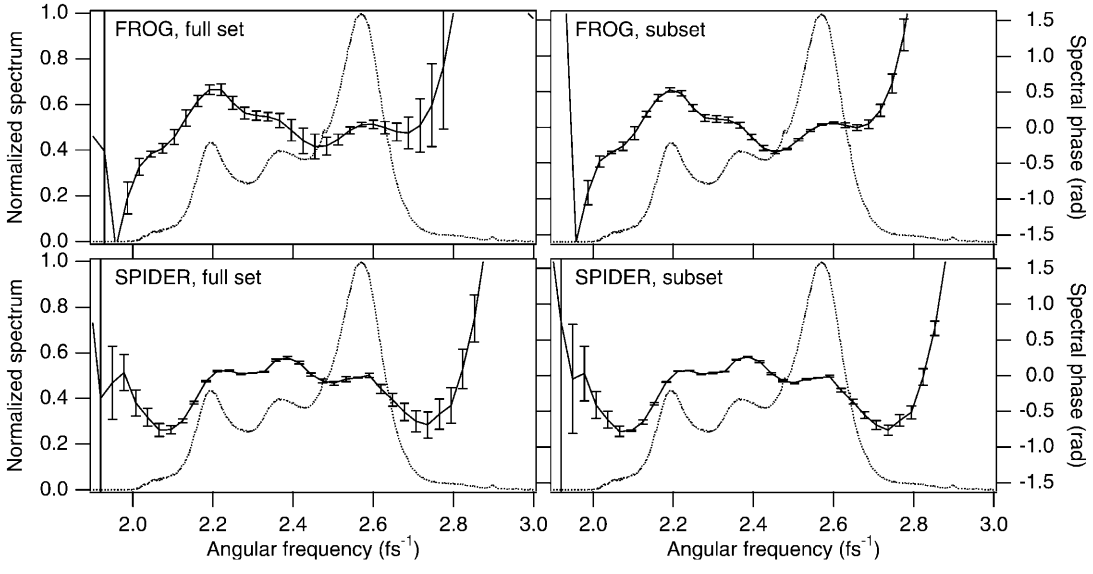

Fig. 9. Variations in the spectral phase obtained with the FROG and SPIDER techniques. The *solid line* represents the average of all reconstructed phases. The pulse spectrum is shown for comparison (*dotted line*)

feature of SPIDER is its simple non-iterative pulse reconstruction procedure.

Combination of different pulse characterization techniques is a useful crosscheck. For example, reconstruction of the interferometric autocorrelation trace from the retrieved pulse shape could confirm the presence of errors in the reconstruction. From the considerations in this paper, we conclude that the potential of both methods is not yet fully utilized. Both SPIDER and FROG should allow for the accurate characterization of pulses in the single-cycle regime.

Acknowledgements. We acknowledge fruitful discussions with I.A. Walmsley, C. Iaconis, R. Trebino, and K.W. DeLong. This work has been supported by the Swiss National Science Foundation.

References

1. G. Steinmeyer, D.H. Sutter, L. Gallmann, N. Matuschek, U. Keller: Science **286**, 1507 (1999)
2. A. Shirakawa, I. Sakane, M. Takasaka, T. Kobayashi: Appl. Phys. Lett. **74**, 2268 (1999)
3. A. Baltuska, Z. Wei, M.S. Pshenichnikov, D.A. Wiersma, R. Szipöcs: Appl. Phys. B **65**, 175 (1997)
4. M. Nisoli, S. Stagira, S.D. Silvestri, O. Svelto, S. Sartania, Z. Cheng, M. Lenzner, C. Spielmann, F. Krausz: Appl. Phys. B **65**, 189 (1997)
5. U. Morgner, F.X. Kärtner, S.H. Cho, Y. Chen, H.A. Haus, J.G. Fujimoto, E.P. Ippen, V. Scheuer, G. Angelow, T. Tschudi: Opt. Lett. **24**, 411 & 920 (1999)
6. D.H. Sutter, G. Steinmeyer, L. Gallmann, N. Matuschek, F. Morier-Genoud, U. Keller, V. Scheuer, G. Angelow, T. Tschudi: Opt. Lett. **24**, 631 (1999)
7. J.L.A. Chilla, O.E. Martinez: Opt. Lett. **16**, 39 (1991)
8. D.J. Kane, R. Trebino: IEEE J. Quantum Electron. **QE-29**, 571 (1993)
9. K.C. Chu, J.P. Heritage, R.S. Grant, K.X. Liu, A. Dienes, W.E. White, A. Sullivan: Opt. Lett. **20**, 904 (1995)
10. J.-K. Rhee, T.S. Sosnowski, A.-C. Tien, T.B. Norris: J. Opt. Soc. Am. B **13**, 1780 (1996)
11. C. Iaconis, I.A. Walmsley: Opt. Lett. **23**, 792 (1998)
12. R. Trebino, K.W. DeLong, D.N. Fittinghoff, J. Sweetser, M.A. Krumbügel, B. Richman: Rev. Sci. Instrum. **68**, 1 (1997)
13. C. Iaconis, I.A. Walmsley: IEEE J. Quantum Electron. **QE-35**, 501 (1999)
14. J. Peatross, A. Rundquist: J. Opt. Soc. Am. B **15**, 216 (1998)
15. A. Baltuska, M.S. Pshenichnikov, D.A. Wiersma: Opt. Lett. **23**, 1474 (1998)
16. Z. Cheng, A. Fürbach, S. Sartania, M. Lenzner, C. Spielmann, F. Krausz: Opt. Lett. **24**, 247 (1999)
17. C.G. Durfee III, S. Backus, H.C. Kapteyn, M.M. Murnane: Opt. Lett. **24**, 697 (1999)
18. L. Gallmann, G. Steinmeyer, D.H. Sutter, N. Matuschek, U. Keller: Opt. Lett. **25**, 269 (2000)
19. L. Gallmann, D.H. Sutter, N. Matuschek, G. Steinmeyer, U. Keller, C. Iaconis, I.A. Walmsley: Opt. Lett. **24**, 1314 (1999)
20. H.A. Haus, J.G. Fujimoto, E.P. Ippen: J. Opt. Soc. Am. B **8**, 2068 (1991)
21. U. Keller, K.J. Weingarten, F.X. Kärtner, D. Kopf, B. Braun, I.D. Jung, R. Fluck, C. Hönninger, N. Matuschek, J. Aus der Au: IEEE J. Sel. Top. Quantum Electron. **2**, 435 (1996)
22. R. Paschotta, J. Aus der Au, G.J. Spühler, F. Morier-Genoud, R. Hövel, M. Moser, S. Erhard, M. Karszewski, A. Giesen, U. Keller: Appl. Phys. B, Suppl. to **70**, 25 (2000)
23. U. Morgner, F.X. Kärtner, S.H. Cho, Y. Chen, H.A. Haus, J.G. Fujimoto, E.P. Ippen, V. Scheuer, G. Angelow, T. Tschudi: Opt. Lett. **24**, 920 (1999)
24. I.D. Jung, F.X. Kärtner, N. Matuschek, D.H. Sutter, F. Morier-Genoud, G. Zhang, U. Keller, V. Scheuer, M. Tilsch, T. Tschudi: Opt. Lett. **22**, 1009 (1997)
25. L. Xu, C. Spielmann, F. Krausz, R. Szipöcs: Opt. Lett. **21**, 1259 (1996)
26. J. Zhou, G. Taft, C.-P. Huang, M.M. Murnane, H.C. Kapteyn, I.P. Christov: Opt. Lett. **19**, 1149 (1994)
27. J. Tignon, M.V. Marquezini, T. Hasche, D.S. Chemla: IEEE J. Quantum Electron. **QE-35**, 510 (1999)
28. A.L. Smirl, X. Chen, O. Buccafusca: IEEE J. Quantum Electron. **QE-35**, 523 (1999)
29. J. Kunde, U. Siegner, S. Arlt, F. Morier-Genoud, U. Keller: Appl. Phys. Lett. **73**, 3025 (1998)
30. J. Kunde, U. Siegner, S. Arlt, G. Steinmeyer, F. Morier-Genoud, U. Keller: J. Opt. Soc. Am. B **16**, 2285 (1999)
31. W.S. Warren, H. Rabitz, M. Dahleh: Science **259**, 1581 (1993)
32. D.J. Tannor, S.A. Rice: J. Chem. Phys. **83**, 5013 (1985)
33. P. Brunner, M. Shapiro: Ann. Phys. Rev. Chem. **43**, 257 (1992)
34. A. Assion, T. Baumert, M. Bergt, T. Brixner, B. Kiefer, V. Seyfried, M. Strehle, G. Gerber: Science **282**, 919 (1998)
35. K.W. DeLong, R. Trebino, J. Hunter, W.E. White: J. Opt. Soc. Am. B **11**, 2206 (1994)
36. A. Baltuska, M.S. Pshenichnikov, D.A. Wiersma: IEEE J. Quantum Electron. **QE-35**, 459 (1999)
37. G. Taft, A. Rundquist, M.M. Murnane, I.P. Christov, H.C. Kapteyn, K.W. DeLong, D.N. Fittinghoff, M.A. Krumbügel, J.N. Sweetser, R. Trebino: IEEE Select. Top. Quantum Electron. **2**, 575 (1996)
38. D.H. Sutter, L. Gallmann, N. Matuschek, F. Morier-Genoud, V. Scheuer, G. Angelow, T. Tschudi, G. Steinmeyer, U. Keller: Appl. Phys. B, Suppl. to **70**, 5 (2000)
39. D.N. Fittinghoff, J.A. Squier, C.P.J. Barty, J.N. Sweetser, R. Trebino, M. Müller: Opt. Lett. **23**, 1046 (1998)
40. D.N. Fittinghoff, A.C. Millard, J.A. Squier, M. Müller: IEEE J. Quantum Electron. **QE-35**, 479 (1999)
41. V.G. Dmitriev, G.G. Gurzadyan, D.N. Nikogosyan: *Handbook of Nonlinear Optical Crystals*, ed. by A.E. Siegman, Opt. Sci. (Springer, Berlin, Heidelberg 1997)
42. S.T. Cundiff, W.H. Knox, E.P. Ippen, H.A. Haus: Opt. Lett. **21**, 662 (1996)
43. L. Gallmann, D.H. Sutter, N. Matuschek, G. Steinmeyer, U. Keller, C. Iaconis, I.A. Walmsley: In Digest of Conference on Lasers and Electro-Optics, paper CFE1 2000
44. K.W. DeLong, R. Trebino, D.J. Kane: J. Opt. Soc. Am. B **11**, 1595 (1994)
45. D.J. Kane: IEEE J. Quantum. Electron. **QE-35**, 421 (1999)
46. K.W. DeLong, C.L. Ladera, R. Trebino, B. Kohler, K.R. Wilson: Opt. Lett. **20**, 486 (1995)
47. C. Froehly, A. Lacourt, J.C. Vienot: Nouv. Rev. Opt. **4**, 183 (1973)
48. M. Takeda, H. Ina, S. Kobayashi: J. Opt. Soc. Am. **72**, 156 (1982)
49. C. Dorrer: Opt. Lett. **24**, 1532 (1999)
50. C. Dorrer: J. Opt. Soc. Am. B **16**, 1160 (1999)
51. C. Dorrer, B. d. Beauvoir, C. Le Blanc, S. Ranc, J.P. Rousseau, J.P. Chambaret, F. Salin: Opt. Lett. **24**, 1644 (1999)
52. T.M. Shuman, M.E. Anderson, J. Bromage, C. Iaconis, L. Waxer, I.A. Walmsley: Opt. Express **5**, 134 (1999)